Numerical Study on Electrode Model for Plasma Simulation of MPD Thruster

IEPC-2011-252

Presented at the 32nd International Electric Propulsion Conference,
Wiesbaden • Germany
September 11 – 15, 2011

K. Kubota[1]
Japan Aerospace Exploration Agency, Chofu, Tokyo, 182-8522, Japan

I. Funaki[2]
Japan Aerospace Exploration Agency, Sagamihara, Kanagawa, 252-5210, Japan

and

Y. Okuno[3]
Tokyo Institute of Technology, Yokohama, Kanagawa, 226-8502, Japan

Abstract: **An electrode model is incorporated into the MHD flow solver for MPD thruster in order to estimate the total discharge voltage. Under the condition of argon propellant of 0.8 g/s, the discharge current is varied in the range of 4 – 6.5 kA. The estimated cathode sheath voltage is about 20 – 25 V regardless of the discharge current, which makes the total discharge voltage much close to the experimental value. At 6 kA, the sheath effect suppresses the current concentration at the anode end, and encourages current distortion near the inlet, which causes the emergence of a compression wave from the cathode root.**

Nomenclature

$\boldsymbol{B}$	=	magnetic field
C	=	thermal velocity
e	=	elementary charge
δE	=	energy exchange via collision
F	=	thrust
$\bar{I}$	=	unit tensor
$\boldsymbol{j}$	=	current density
J	=	total discharge current
k	=	Boltzmann constant
m	=	mass of particle
n	=	number density
p	=	pressure
r	=	radial coordinate
T	=	temperature
$\boldsymbol{u}$	=	velocity
U	=	internal energy
V	=	voltage

[1] Researcher, Aerospace Research and Development Directorate, kubota.kenichi@jaxa.jp
[2] Associate Professor, Institute of Space and Astronautical Science, funaki@isas.jaxa.jp
[3] Professor, Department of Energy Sciences, yokuno@es.titech.ac.jp

V_i = ionization energy
z = axial coordinate
α = ionization degree
θ = azimuthal coordinate
λ = thermal conductivity
μ_0 = permeability in vacuum
ρ = mass density
σ = electrical conductivity
$\bar{\tau}$ = viscous tensor
φ_w = work function

Subscripts

a : anode
b : bulk
c : cathode
e : electron
h : heavy particle
hc : hot cathode
n : neutral
pb : boundary between bulk plasma and pre-sheath region
sh : sheath
tot : total

I. Introduction

Recently, desirable power range for an electric propulsion device has been getting larger in accordance with expanding scales of new and ambitious space missions. A magnetoplasmadynamic thruster (MPDT) is known as a representative high-power electric propulsion device suitable for such a large scale mission. An MPDT accelerates ionized propellant with the Lorentz force driven by discharge current and induced magnetic field as shown in Fig. 1. In spite of the many experimental and theoretical efforts on the performance improvement, detailed phenomena within the thruster and the definite guideline for the electrode design and working conditions have not yet been specified.

Experimental studies have provided a lot of important data of MPDTs such as thrust efficiency.[1] On the other hand, in the numerical simulation, there still remains an essential problem of predicting thrust efficiency. In a calculation, thrust and voltage have to be predicted for evaluation of thrust efficiency, because a discharge current is set as an input parameter. Most numerical studies showed that the thrust-current characteristics agree well with the experimental data, but remains in a difficult situation for prediction of total discharge voltage due to the uncertainties of sheath voltage drop on the electrodes, which results in an obstacle to quantitative discussion about thrust efficiency.

The purpose of this study is to develop an electrode model (EM) applicable to the flow solver for the self-consistent prediction of total discharge voltage. The EM is based on the model developed by Fujita for weakly ionized plasma in a DC-Arcjet.[2] Since the plasma in an MPDT is generally highly or fully ionized, the EM for a DC-Arcjet is extended for the plasma with arbitrary ionization degree. The developed EM is incorporated into our flow

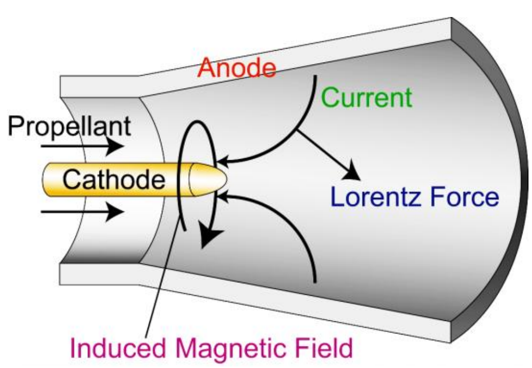

Figure 1. Principle of MPD Thruster.

solver as a boundary condition of the plasma, which enables us to discuss the plasma flow in association with sheath voltage and thrust efficiency. The influence of the EM on the flow field, especially electron temperature and electron number density, is also examined.

II. Numerical Modeling

A. Thruster Geometry

The flow under consideration is assumed to be axisymmetric. The thruster consists of a flared anode and a short cathode. Each radius of the anode and the cathode is 14 mm and 4 mm at the inlet where the propellant is uniformly injected. The axial length of the cathode and the anode is 13 mm, and 45 mm, respectively. At the outlet of the thruster (z = 45 mm), the anode is 27 mm in radius, and an insulator is located around the anode.

B. Basic Equations

In this study, argon is used as a propellant, and non-equilibrium singly ionization processes are simulated.[3] The heavy particles (ion, neutral) and the electrons are assumed to be thermally non-equilibrium. The basic equations are conservation equations of mass, momentum, energy (heavy particles, electrons), and the induction equation. The induction equation is used to determine the azimuthal induced magnetic field.

Continuity equation

$$\frac{\partial \rho}{\partial t} + \nabla \cdot (\rho \boldsymbol{u}) = 0 \tag{1}$$

Continuity equation for ion

$$\frac{\partial \rho_i}{\partial t} + \nabla \cdot (\rho_i \boldsymbol{u}) = \dot{\rho}_i \tag{2}$$

Momentum conservation

$$\frac{\partial \rho \boldsymbol{u}}{\partial t} + \nabla \cdot \left[\rho \boldsymbol{u}\boldsymbol{u} + p\bar{I}\right] = \boldsymbol{j} \times \boldsymbol{B} + \nabla \cdot \bar{\tau} \tag{3}$$

Energy conservation of heavy particles

$$\frac{\partial E_h}{\partial t} + \nabla \cdot (E_h + p)\boldsymbol{u} = p_e \nabla \cdot \boldsymbol{u} + \boldsymbol{u} \cdot (\boldsymbol{j} \times \boldsymbol{B}) - \nabla \cdot \boldsymbol{q}_h + \nabla \cdot (\bar{\tau}\boldsymbol{u}) + \delta E \tag{4}$$

Internal energy conservation of electrons

$$\frac{\partial U_e}{\partial t} + \nabla \cdot U_e \boldsymbol{u} = -p_e \nabla \cdot \boldsymbol{u} + \frac{\boldsymbol{j}^2}{\sigma} - \nabla \cdot \boldsymbol{q}_e - \delta E - eV_i \tag{5}$$

Induction equation

$$\frac{\partial \boldsymbol{B}}{\partial t} - \nabla \times (\boldsymbol{u} \times \boldsymbol{B}) = -\nabla \times \left[\frac{1}{\mu_0 \sigma} \nabla \times \boldsymbol{B} + \frac{1}{\mu_0 e n_e} (\nabla \times \boldsymbol{B}) \times \boldsymbol{B}\right] \tag{6}$$

where

$$E_h = \frac{1}{2}\rho \boldsymbol{u}^2 + \frac{3}{2} n_h k T_h, \quad U_e = \frac{3}{2} n_e k T_e \tag{7}$$

The right hand side of Eq. (2) represents an ion production rate in which it is assumed that ionization is driven only by electron impact. Lotz formula is used as a forward reaction rate, and a backward reaction rate is determined from an equilibrium constant. The δE denotes the rate of energy exchange via elastic collisions between heavy particles and electrons. The heat fluxes can be given as follows.

$$\boldsymbol{q}_h = -\lambda_h \nabla T_h, \quad \boldsymbol{q}_e = -\lambda_e \nabla T_e - \frac{5k}{2e} T_e \boldsymbol{j} \tag{8}$$

To close the system of equations, the Ampere's law and the equation of state are included in the formulation.

$$\boldsymbol{j} = \frac{\nabla \times \boldsymbol{B}}{\mu_0} \tag{9}$$

$$p = p_h + p_e = n_h k T_h + n_e k T_e \tag{10}$$

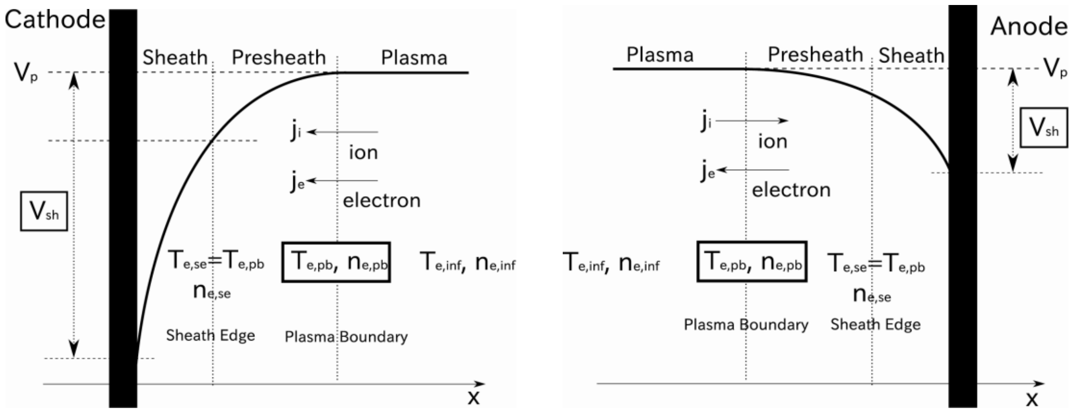

Figure 2. Conceptual diagram of electrode model (The x-coordinate is set from the cathode to the anode, i.e. a vector having a minus value points in the cathode direction.).

The convective terms in Eq. (1)-(6) are discretized with second-order TVD Lax-Friedrich scheme, and the second-order derivatives are evaluated with the central difference formula.[4] In the time integration, the local time step technique is used to accelerate convergence.

C. Electrode Model

The conceptual diagram of our EM is shown in Fig. 2. The x-coordinate is set from the cathode to the anode, which means that the vectors in the direction of the cathode have a minus value. It is assumed that an ion-rich sheath is formed on the anode, which will be appropriate for a relatively moderate discharge condition. In this model, the electron temperature, the electron number density, and the sheath voltage at the plasma boundary (PB) are determined by solving equations of current conservation, electron energy conservation, and relation on ion diffusion.

The total current density j_{tot} is equal to the sum of ion current j_i and electron current j_e.

$$j_{tot} = j_i + j_e = j_i + j_{hc} + j_{th} \exp\left(-\frac{eV_{sh}}{kT_{e,pb}}\right) \tag{11}$$

where

$$j_i = \pm e n_{e,se}\sqrt{\frac{kT_{e,se}}{m_h}} = \pm e \exp\left(-\frac{1}{2}\right) n_{e,pb}\sqrt{\frac{kT_{e,pb}}{m_h}} \tag{12}$$

$$j_{hc} = -AT_c^2 \exp\left(-\frac{e\varphi_{Th-W}}{kT_c}\right) \qquad \text{(only for cathode)} \tag{13}$$

$$j_{th} = \mp\frac{1}{4} e n_{e,pb} C_{e,pb} \tag{14}$$

Here, V_{sh} should be interpreted as V_c on the cathode or V_a on the anode. Note that V_{sh} is defined as a positive value on both electrodes. The ion current is assumed to be the ion saturation current, i.e. the ions are assumed to inflow into the sheath region with Bohm velocity at PB. The electron current consists of the electron flux from a hot cathode and the electron inflow from the bulk plasma into the sheath region. The electron current from a hot cathode is given from the Richardson-Dashman formula of Eq.(13), in which a factor (A) and a work function (φ_{Th-W}) are set to 3×10^4 A/m^{2}K^2 and 2.62 eV respectively to assume thoriated tungsten as the cathode material.[5] As the sign of the Eqs. (12) and (14), the upper and lower signs are chosen for the anode and cathode, respectively.

The energy flux of the electrons toward the cathode from the bulk region can be given as follows.

$$-\lambda_e \left.\frac{\partial T_e}{\partial x}\right|_{pb} = -\frac{1}{4} n_{e,pb} C_{e,pb} \exp\left(-\frac{eV_{sh}}{kT_{e,pb}}\right)\left(eV_{sh} + 2kT_{e,pb}\right) \tag{15}$$

On the other hand, the electron energy balance on the anode can be expressed as follows.

$$-\frac{5k}{2e} T_{e,pb} j_{tot} - \lambda_e \left.\frac{\partial T_e}{\partial x}\right|_{pb} = \frac{1}{4} n_{e,pb} C_{e,pb} \exp\left(-\frac{eV_{sh}}{kT_{e,pb}}\right)\left(eV_{sh} + 2kT_{e,pb}\right) \tag{16}$$

The ion diffusion velocity for arbitrary ionization degree can be derived as[6]

$$\boldsymbol{U}_i = \frac{1}{(1+D)en_e}\left[D\boldsymbol{j}_{tot} + \frac{\rho_n}{\rho}\mu_{in}\left(-\nabla(p_i + p_e) + \frac{\rho_i}{\rho}\nabla p\right)\right] \tag{17}$$

where

$$D = \frac{\rho_e}{\rho} + \frac{\rho_n}{\rho}\frac{\mu_{in}}{\mu_e}\left(1 - \frac{\nu_{ie}}{\nu_{eh}}\right) \tag{18}$$

The ion diffusion current en_eU_i at PB should be equal to the ion saturation current as assumed above.

$$j_{i,pb} = en_{e,pb}U_{i,pb} \tag{19}$$

The Eqs.(11),(15),(16), and (19) are numerically solved with regard to $T_{e,pb}$, $n_{e,pb}$, V_{sh} with the input parameters of j_{tot}, and heavy particle temperature (=electrode temperature). In addition, some parameters at infinity such as electron temperature, pressure, ionization degree should be given, for which the physical value at the closest grid point to the each grid point on electrodes is utilized in the actual flow calculation.

Figure 3 shows the influence of current density on relation between cathode sheath and cathode temperature under the condition of $T_{e,\text{inf}}$ = 5 eV, p_{inf} = 3 kPa, α = 1. The result indicates that, for high current density, the model does not have a solution below a certain cathode temperature. This tendency can be understood by rewrite Eq. (11) as

$$V_{sh} = -\frac{kT_{e,pb}}{e}\ln\left(\frac{j_{tot} - j_i - j_{hc}}{j_{th}}\right) \tag{20}$$

where note that j_{tot}, j_i, and j_{hc} are negative values and j_{th} is a positive value in this formulation. For finite V_{sh}, $|j_{tot}| < |j_i + j_{hc}|$ is required. When the cathode temperature is decreased from adequately high temperature, $|j_{hc}|$ converges to zero as seen from Eq. (13). Consequently, if $|j_{tot}| < |j_i|$, V_{sh} can be kept finite, but if $|j_{tot}| > |j_i|$, V_{sh} reaches an infinite value at a cathode temperature satisfying $j_{tot} - j_i - j_{hc} = 0$.

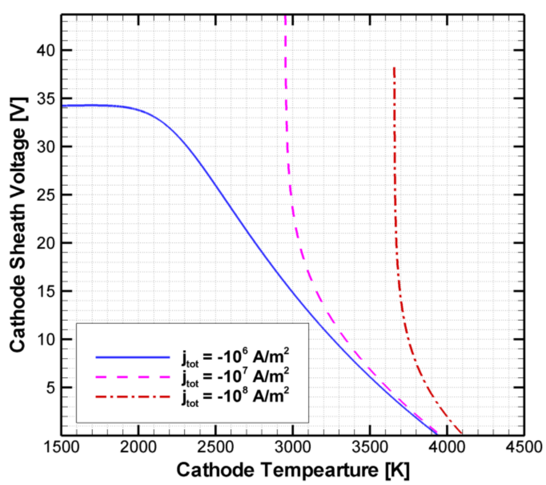

Figure 3. Influence of current density on relation between cathode sheath and cathode temperature. ($T_{e,\text{inf}}$ = 5 eV, p_{inf} = 3 kPa, α = 1)

On the anode surface, Eqs. (11), (16), and (19) are numerically solved with regard to $T_{e,pb}$, $n_{e,pb}$, V_{sh}, in which an anode temperature of 1,300 K is assumed, and j_{hc} is set at zero. On the cathode surface, firstly, Eqs. (11), (15), and (19) are solved with regard to $T_{e,pb}$, $n_{e,pb}$, V_{sh} at the cathode root (z = 0 mm), in which the cathode temperature is gradually increased from an initial value until a proper solution of the non-linear equations can be found. Second, the total discharge voltage V_{tot} defined by the sum of the cathode sheath voltage V_c, anode sheath voltage V_a, and the voltage drop in the bulk plasma V_b is calculated at the inlet as follows,

$$V_{tot} = (V_c + V_b - V_a)_{inlet} \tag{21}$$

where V_a is defined as a positive value. Third, for the each remained part of the cathode surface, the cathode sheath voltage is determined from the total discharge voltage, anode sheath voltage, and the bulk voltage drop as,

$$V_c(z) = V_{tot} - V_b(z) + V_a(z) \tag{22}$$

where z is the axial coordinate. Lastly, the cathode temperature, $T_{e,pb}$, and $n_{e,pb}$ can be calculated at remained each part of the cathode from Eqs. (11), (15), (19) by the use of $V_{sh} = V_c(z)$. These procedures can ensure the equipotential condition between the electrodes as well as determine the distribution of the cathode surface temperature self-consistently.

D. Calculation Conditions

The calculation conditions are tabulated in Table 1. The mass flow rate is kept constant, and the discharge current is varied from 4 kA to 6.5 kA with 0.5 kA increments. With this mass flow rate, the theoretical critical current, which is known as an indicator of minimum discharge current causing voltage oscillation, is about 6 kA.

The heavy particle temperature is set to the same value as the electrodes. The electron temperature and the electron number density on the walls are determined from the EM. The electron thermal flux provided by the model is employed on the walls. For the velocity, non-slip condition is imposed on the walls. The magnetic field at the inlet is determined from Ampère's law.

$$B_\theta = -\frac{\mu_0 J}{2\pi r} \tag{23}$$

The existence of a sheath also influences the boundary condition of the azimuthal induced magnetic field. Since the boundary of the computational domain corresponds to the boundary between plasma and the sheath region, a pertinent boundary condition should be

$$E_\xi = -\frac{dV_{sh}}{d\xi} \tag{24}$$

where ξ denotes a coordinate along an electrode. Equation (24) can be converted into the function of the induced magnetic field with the aid of generalized Ohm's law and Ampère's law. The nonlinear equation with regard to the induced magnetic field is numerically solved on the electrode.

Table 1. Calculation Conditions.

Propellant	Argon
Mass flow rate (g/s)	0.8
Discharge current (kA)	4 - 6.5
Inlet heavy particle temperature (K)	5000
Inlet electron temperature (K)	10000
Inlet ionization degree	0.1
Heavy particle temperature on anode (K)	1300

III. Results and Discussion

A. Comparison of Performance with Experimental Data

First of all, in order to validate the numerical results, the thrust and discharge voltage are compared with the experimental result obtained by Nakata.[7] The thrust can be defined as the sum of the aerodynamic force, electromagnetic force (EMF), and viscous loss. The theoretical EMF is given by Maecker's formula.[8]

$$F_{EMF} = \frac{\mu_0 J^2}{4\pi}\left(\ln\frac{r_a}{r_c} + a\right), \qquad 0 < a < 3/4 \tag{25}$$

Here, r_a and r_c are the radius of the anode and the cathode, respectively. Figure 4 is the numerical and experimental results of the thrust-current characteristics, and indicates that the calculated thrust agrees well with the experimental data. From the calculated EMF, which is estimated by the integration of the blowing force, the ratio of the EMF to the total thrust amounts to about 68% at J = 6.5 kA.

Figure 5 is the voltage-current characteristics. The averaged values of the voltage within the bulk (V_b), cathode sheath voltage (V_c), and anode sheath voltage (V_a), which are defined as follows, are also plotted.

$$V_{b,ave} = \int_b \boldsymbol{j}\cdot\boldsymbol{E}dV \Big/ J, \qquad V_{c,ave} = \int_c |j_n| V_c dS \Big/ J, \qquad V_{a,ave} = -\int_a |j_n| V_a dS \Big/ J \tag{26}$$

Note that the $V_{a,ave}$ is defined as a negative value, because the ion-rich sheath is assumed on the anode. The result shows that the cathode sheath voltage is around 20 – 25 V regardless of the discharge current. This tendency agrees with the experimental data measured with zero-limit approximating method.[9] $|V_{a,ave}|$ is a few volts, and is gradually increased with discharge current. Owing to the cathode sheath, the total voltage becomes well close to the experimental value, which will suggests the validity of the developed EM. It can be seen that the increase in the voltage with discharge current is mainly attributed to the increase in V_b which is considered to result from the Hall effect.

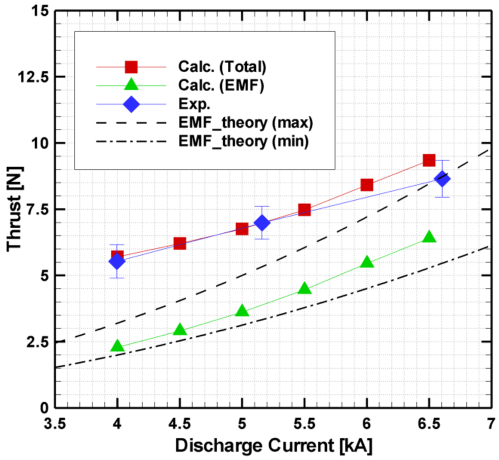

Figure 4. Thrust-Current Characteristics.

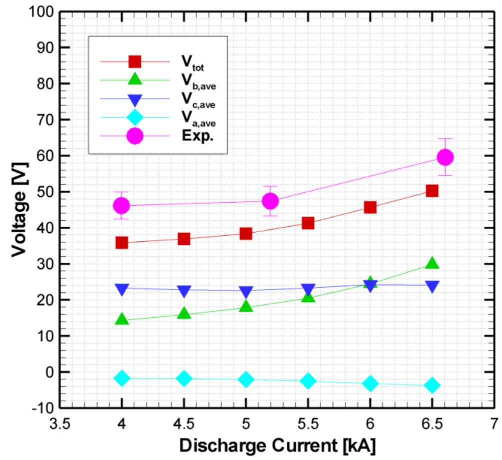

Figure 5. Voltage-Current Characteristics.

B. Current Path and Sheath Voltage

The influence of the EM on the current path is discussed. Figure 6 shows the current paths of J = 4, 6 kA with and without EM. In the case without the EM, the thermal conduction with regard to the electrons is ignored. The labels denote the ratio of the current, flowing downstream viewed from the contour line, to the total discharge current. In addition, the axial profile of the the anode sheath voltage and cathode sheath voltage and cathode temperature are illustrated in Fig. 7 and Fig. 8, respectively.

When J = 4 kA, there is little influence of the EM on the current path, but the current near the anode slightly shifts toward the downstream region. This is due to windward electric field produced by the gradually increased anode sheath voltage in the range of z = 0 – 10 mm as shown in Fig. 7. The windward electric field leads to leeward Coulomb force for the electrons flowing into the anode, which results in the current shift toward the downstream region. On the nozzle part of z = 6 – 45 mm, in spite of the gradually decreasing anode sheath voltage, the sheath seems to have little influence on the current path due to the small slope of the anode sheath variation. On the cathode surface, the current slightly concentrates on the convex point of the cathode (z = 6 mm), which is encouraged by the concave profile of the cathode sheath voltage at that point as shown in Fig. 8.

On the other hand, when J = 6 kA, notable influence of the EM can be confirmed. On the anode surface, the current tends to shift downstream in the range of z = 0 – 20 mm by incorporating the EM for the same reason as the case of J = 4 kA. With the EM, the current concentration at anode end (z = 45 mm), which results from the Hall effect,[3] is suppressed due to the leeward electric field produced by the decreasing anode sheath voltage in the range of z > 25 mm. The spatial oscillation of the anode sheath voltage around z = 20 mm is related with the spatially disturbed current density. On the cathode surface, the cathode sheath voltage a minimum point near the inlet and is gradually increased, which encourages the current shift toward upstream part on the cathode. The gradual increase in the cathode sheath is considered to be encouraged by the Hall effect. Since the Hall effect induces the obliquely distorted current profile, the current is also shifted toward upstream near the cathode surface. As the current concentrates at a certain point, the voltage drop of the bulk plasma is increased at that position. Thus the cathode sheath voltage is decreased near the inlet in accordance with Eq. (22), and is gradually increased in the downstream region where the voltage drop of the bulk plasma is lower than that near the inlet.

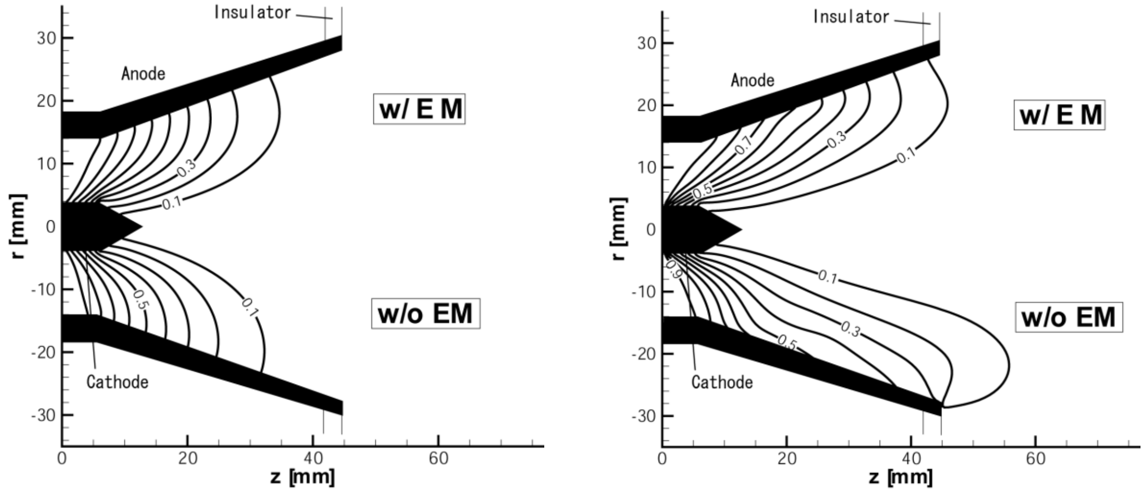

(a) 4 kA (b) 6 kA

Figure 6. Current Path, (Ar, 0.8 g/s).

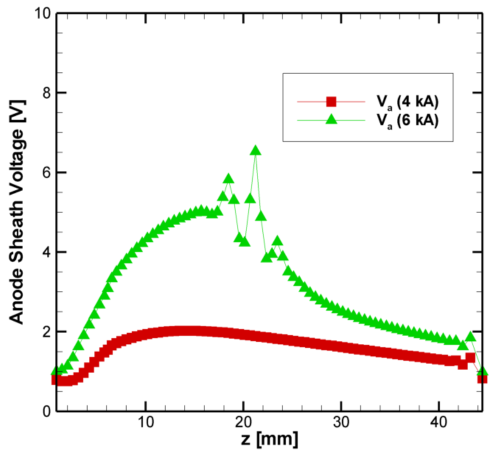

Figure 7. Anode Sheath Voltage.

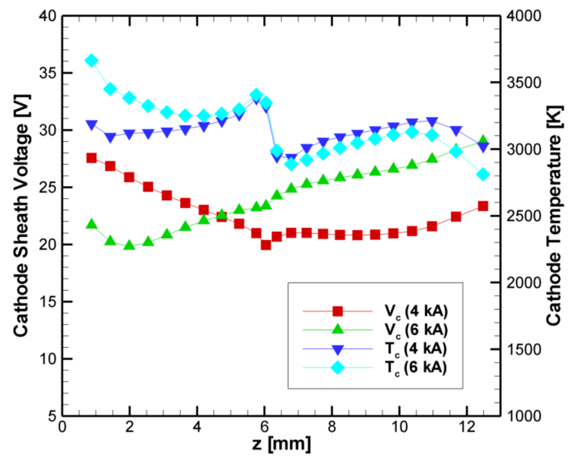

Figure 8. Cathode Sheath Voltage and Cathode Temperature.

C. Flow Field

In order to understand the sheath profile in terms of the flow field, the electron temperature and electro number density are shown in Figs. 9 and 10. With the EM, the electron temperature is decreased near the anode surface due to the consideration of the electron thermal conduction. The electron temperature on the anode has a peak around z = 20 mm, which will be a reason for the peak of the anode sheath voltage around the same part. Near the cathode, the electron temperature is increased around the point on which the current concentrates. The electron number density for J = 4 kA is not so affected by the EM, but there is a notable difference in the case of J = 6 kA. The encouraged distortion of the current path near the inlet increases the radial Lorentz force, which leads to the strong compression wave propagating from the cathode root, and also results in the low density near the anode around z = 20 mm. This density depletion may be related with the current oscillation and hence oscillation of the anode sheath voltage.

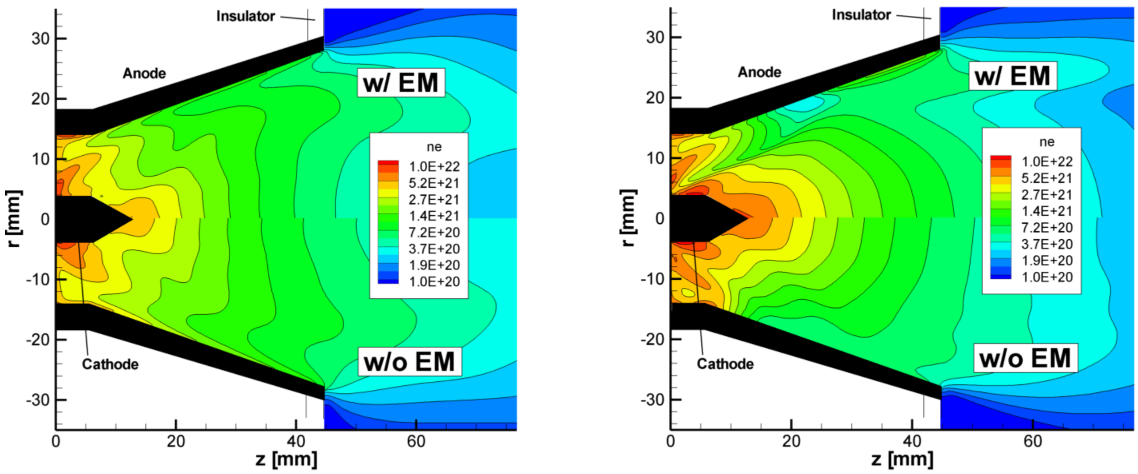

(a) 4 kA (b) 6 kA

Figure 9. Electron Number Density, m^{-3}, (Ar, 0.8 g/s).

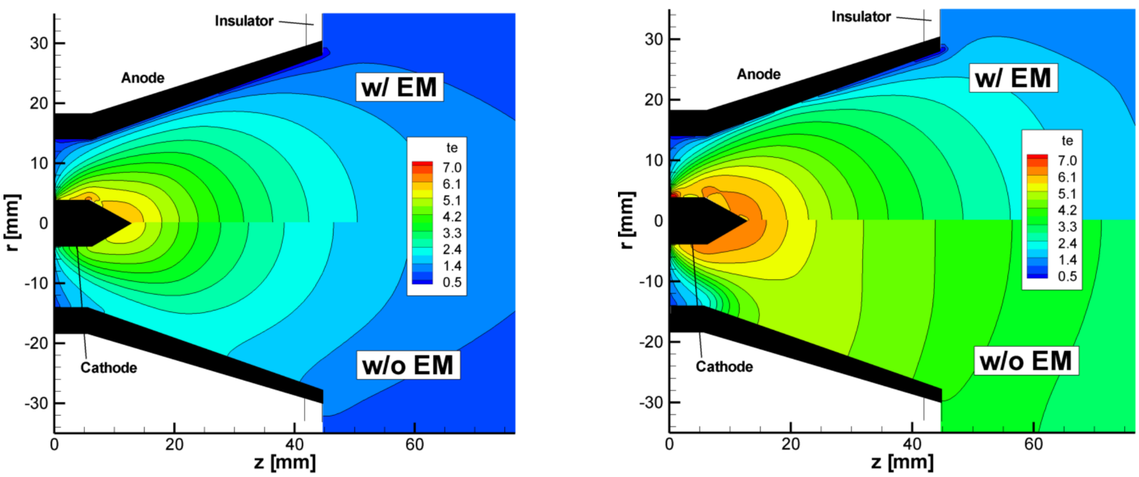

(a) 4 kA (b) 6 kA

Figure 10. Electron Temperature, eV (Ar, 0.8 g/s).

IV. Conclusion

In order to estimate total discharge voltage of an MPD thruster, an electrode model is incorporated into the MHD flow solver, which enables us to estimate the sheath voltage on the electrodes. The propellant is argon, and the discharge current is varied under a constant mass flow rate of 0.8 g/s. The thrust agrees well with the experimental data, and the discharge voltage becomes much close to the experimental results. The averaged cathode sheath voltage is about 20 – 25 V, and is not strongly dependent on the current. Without the electrode model, the current tends to concentrate on the anode end due to the Hall effect, but this is suppressed by considering the electrode model due to the leeward electric field produced by the axially decreasing anode sheath voltage. The oblique current distortion is encouraged by the EM, which causes the compression wave propagating from the cathode root.

References

[1] Lapointe, M. R., Strzempkowski, E., and Pencil, E., “High Power MPD Thruster Performance Measurements,” AIAA Paper 2004-3467, 2004.

[2] Fujita, K., and Arakawa, Y., “Performance Computation of a Low-Power Hydrogen Arcjet,” *Journal of Propulsion and Power*, Vol. 15, No. 1, pp. 144-150, 1999.

[3] Kubota, K., I. Funaki, and Y. Okuno, “Numerical Study of Plasma Behavior in a Magnetoplasmadynamic Thruster Around Critical Current,” *Journal of Propulsion and Power*, Vol. 25, No. 2, pp. 397-405, 2009.

[4] Tóth, G., and Odstrčil, D., “Comparison of Some Flux Corrected Transport and Total Variation Diminishing Numerical Schemes for Hydrodynamic and Magnetohydrodynamic Problems,” *J. Comput. Phys.*, Vol. 128, pp. 82-100, 1996.

[5] Lu, J., Krier, H., Burton, R. L., and Goodfellow, K. D., “Cathode Sheath Voltage Models for Hydrazine Arcjets,” *Journal of Thermophysics and Heat Transfer*, Vol. 12, No. 2, pp. 230-238, 1998.

[6] Mitchner, M., Kruger, C. H., *Partially Ionized Gases*, John Wiley & Sons, Inc., New York, 1973.

[7] Nakata, D., Toki, K., Funaki, I., Shimizu, Y., Kuninaka, H., Arakawa, Y., “Experimental Verification for the Nozzle Shape Optimization of the Self-Field MPD Thruster,” IEPC-2005-163, 2005.

[8] Jahn, R. G., *Physics of Electric Propulsion*, McGraw-Hill, New York, 1968.

[9] Nakata, D., Toki, K., Funaki, I., Shimizu, Y., Kuninaka, H., and Arakawa, Y., “Experimental measurement of Total Sheath Fall Voltage in an MPD thruster,” AIAA-2008-4635, 2008.